

## Enhanced Corrosion Resistance of AZ31B Magnesium Alloy by Cooperation of Rare Earth Cerium and Stannate Conversion Coating

Lei Li<sup>1</sup>, Qing Qu<sup>2,\*</sup>, Zhiwen Fang<sup>2</sup>, Lin Wang<sup>2</sup>, Yunwei He<sup>2</sup>, Rui Yuan<sup>2</sup>, Zhongtao Ding<sup>2</sup>

<sup>1</sup> Laboratory for Conservation and Utilization of Bio-Resources, Yunnan University, Kunming 650091, China

<sup>2</sup> School of Chemical Science and Technology, Yunnan University, Kunming 650091, China

\*E-mail: [quqing58@yahoo.com.cn](mailto:quqing58@yahoo.com.cn)

Received: 12 October 2012 / Accepted: 9 November 2012 / Published: 1 December 2012

---

The optimal conditions for formation of single stannate or cerium conversion coatings formed on AZ31B magnesium were selected through orthogonal experiment analysis, and then anticorrosive composite film on AZ31B magnesium alloy by a combination process of rare earth cerium and stannate was investigated for the first time by Tafel polarization and electrochemical impedance spectroscopy (EIS). The film formed by single rare earth cerium or stannate can correspondingly retard the corrosion of AZ31B alloy. However, combination of rare earth cerium and stannate further enhances the corrosion resistance clearly; the composite coating has much higher corrosive resistance than that by each single component. Additionally, the corrosion resistance of the composite film increases with increasing immersion time. A comparison of SEM and XRD results further indicates that the composite coating shows multilayer film composed of cerium oxide compound, magnesium stannate compounds and magnesium hydroxide.

---

**Keywords:** Magnesium alloy, cerium ion, stannate, composite film, corrosion resistance

### 1. INTRODUCTION

Magnesium is one of the lightest materials and an attractive metal because of its high stiffness and low density. Magnesium alloys as functional materials are used in the aerospace, automotive application and electronic industries [1,2]. However, magnesium alloys have low corrosion potential and easily corrodes, which limits their extensive utilization in these fields. Therefore, development of appropriate surface treatments such as physical vapor depositions, anodic oxidations, and chemical conversions has led to improvement of the corrosion resistance of magnesium alloys [3,4]. Various chemical conversions have been used as surface treatments of magnesium alloys because of their

simple and low cost process relative to other surface techniques [5-7]. Among various chemical conversions, chromate systems show excellent corrosion-inhibition property [8]. However, the chromate treatment is being eliminated due to its high toxicity and carcinogenicity [9]. Therefore, it is urgent to develop new environmental-friendly conversion treatments for magnesium alloys.

Stannate conversion coatings and rare earth conversion coatings, which are considered to be environmentally acceptable, have been developed to protect conventional magnesium alloys [10-19]. Rudd et al.[10] investigated the corrosion behaviour of magnesium substrates pretreated with cerium, lanthanum and praseodymium conversion films, their results showed that the conversion layers reduced the dissolution of magnesium in a pH 8.5 buffer solution. Dabalà et al. [11] reported that an excess of hydrogen peroxide concentration increased the amount of Ce(IV) species included in the conversion layer and decreased the corrosion resistance. Montemor et al.[12] studied the effect of various Ce(III) salts on the corrosion resistance of cerium conversion film on AZ31 magnesium alloy, their results indicated that the corrosion protection efficiency was related with the anion present in the cerium salt. Heakal et al. [13] also used Ce (III) to enhance the corrosion resistance of AM60 in NaCl solution. Furthermore, stannate coatings have been formed on magnesium and its alloys by the simple immersion method [14-16]. In those studies, the process of coating formation and the composition of the solution and the immersion parameters have been investigated in detail. To date, there are still some limitations existing in the stannate or rare earth conversion coatings, the corrosion resistances of them are rather lower, they should be utilized in combination with other surface treatments [17]. In order to improve the corrosion resistance of rare earth conversion, Salman et al. [18] tried to add  $\text{Ca(OH)}_2$  and  $\text{Al(NO}_3)_3$  to  $\text{Ce(NO}_3)_3$  solution, their results indicated that addition of  $\text{Ca(OH)}_2$  and  $\text{Al(NO}_3)_3$  to cerium-based solution could enhance the anticorrosion property of the film. Elsentriecy et al.[19] tried to improve the corrosion resistance of stannate chemical conversion coatings on AZ91D magnesium alloy by using potentiostatic technique. However, all the results still are not satisfactory. Thus, it is interesting to further improve the corrosion resistance of stannate conversion coatings and rare earth conversion coatings.

The objective of this investigation is to develop an anticorrosive composite film by a combination process of rare earth cerium (III) and stannate. It is also aimed to predict the corrosion resistance of the composite film coated AZ31B in 3.5% NaCl solution by Tafel polarization and electrochemical impedance spectroscopy (EIS). Scanning electron microscopy (SEM) and X-ray diffraction (XRD) were also used to observe microstructures and characterize the anticorrosive film coated AZ31B magnesium alloy.

## 2. EXPERIMENTAL

### 2.1. Materials

Magnesium alloy AZ31B (Al 3.05%, Zn 0.99%, Mn 0.28%, Fe 0.003%, Si 0.025%, Cu 0.002%, Ni 0.0049% and Mg balance.) with a size of  $20 \times 20 \times 5$  mm was used as the substrate.

Sodium stannate trihydrate ( $\text{Na}_2\text{SnO}_3 \cdot 3\text{H}_2\text{O}$ ), cerium nitrate ( $\text{Ce}(\text{NO}_3)_3$ ), sodium hydroxide ( $\text{NaOH}$ ), sodium pyrophosphate decahydrate ( $\text{Na}_4\text{P}_2\text{O}_7 \cdot 10\text{H}_2\text{O}$ ), sodium acetate trihydrate ( $\text{CH}_3\text{COONa} \cdot 3\text{H}_2\text{O}$ ), sodium chloride ( $\text{NaCl}$ ) and hydrogen peroxide ( $\text{H}_2\text{O}_2$ ) used were of analytical grade. All solutions were prepared from distilled water.

## 2.2. Film preparation

The samples were abraded with emery paper up to 1200 grade, washed with distilled water and cleaned in acetone ultrasonically for 10 min and finally dried in a stream of air.

**Table 1.** The experiment variables design for cerium and stannate coating.

Type	Variable	Level			
		1	2	3	
Cerium coating	A	$\text{Ce}(\text{NO}_3)_3 \cdot 6\text{H}_2\text{O}$ (mol/L)	0.005	0.01	0.015
	B	$\text{H}_2\text{O}_2$ (mL/L)	50	100	150
	C	Temperature ( $^\circ\text{C}$ )	40	50	60
Stannate coating	A	$\text{Na}_2\text{SnO}_3$ (mol/L)	0.05	0.10	0.20
	B	$\text{NaOH}$ (mol/L)	0.10	0.20	0.30
	C	$\text{Na}_4\text{P}_2\text{O}_7 \cdot 10\text{H}_2\text{O}$ (mol/L)	0.04	0.08	0.10
	D	Temperature ( $^\circ\text{C}$ )	50	70	90

**Table 2.** Orthogonal experimental design table for single cerium coating

Sequence number	Experimental Variable and level			$i_{corr}$ ( $\mu\text{A cm}^{-2}$ )
	A	B	C	
1	1	1	1	916.6
2	1	2	2	966.7
3	1	3	3	757.5
4	2	1	2	881.4
5	2	2	3	691.2
6	2	3	1	583.2
7	3	1	3	975.0
8	3	2	1	628.3
9	3	3	2	786.5

The optimal conditions for formation of single stannate conversion coatings or cerium conversion coatings were selected through orthogonal experimental analysis. For cerium conversion coatings,  $\text{Ce}(\text{NO}_3)_3$ ,  $\text{H}_2\text{O}_2$  and temperature were selected as the main effect factors, each factor had three different levels (table 1) ; for stannate conversion coating,  $\text{Na}_2\text{SnO}_3 \cdot 3\text{H}_2\text{O}$ ,  $\text{Na}_4\text{P}_2\text{O}_7 \cdot 10\text{H}_2\text{O}$ ,

NaOH and temperature were selected as the main effect, each factor also had three different levels (table 1), in addition, concentration of  $\text{CH}_3\text{COONa}\cdot 3\text{H}_2\text{O}$  was fixed at  $0.1 \text{ mol L}^{-1}$ . In order to reduce the number of mixes, the experiments were designed according to the orthogonal experimental table of  $L_9 (3^4)$  which were respectively shown in table 2 and 3.

**Table 3.** Orthogonal experimental design table for stannate coating (concentration of  $\text{CH}_3\text{COONa}\cdot 3\text{H}_2\text{O}$  is  $0.1 \text{ mol L}^{-1}$ )

Sequence number	Experimental Variable and level				$i_{corr} (\mu\text{A cm}^{-2})$
	A	B	C	D	
1	1	1	1	1	695.1
2	1	2	2	2	588.0
3	1	3	3	3	573.0
4	2	1	2	3	151.9
5	2	2	3	1	387.1
6	2	3	1	2	286.3
7	3	1	3	2	191.5
8	3	2	1	3	206.6
9	3	3	2	1	580.6

Based on the orthogonal experiment analysis, the rare earth bath and stannate bath were initially determined respectively. The composite film coated AZ31B was first performed in rare earth bath and then immersed in stannate bath.

### 2.3. SEM and XRD study

The anticorrosive surfaces were dried with a cold blower, and then used for Holland yielding XL30 ESEM-TMP scanning electron microscopy detection. The X-ray diffraction measurements were carried out by using Model D/max-3B diffractometer complying with a scanning step of  $0.05^\circ$ .

### 2.4. Electrochemical measurements

The working electrodes were embedded in PVC holder using epoxy resin with a square surface of  $4.0 \text{ cm}^2$ . Before electrochemical measurements, the working electrodes were pretreated to form anticorrosive films based on film preparation. A three-electrode system including a working electrode, an auxiliary electrode and a reference electrode was used for electrochemical measurements in 250 mL solution. Auxiliary electrode was a platinum foil and the reference electrode was a saturated calomel electrode (SCE) with a Luggin capillary positioned close to the working electrode surface in order to minimize ohmic potential drop. EIS was carried out in a frequency range of 100 kHz to 0.1 Hz using a 10 mV peak-to-peak voltage excitation. Tafel polarization scan was carried out by polarizing to  $\pm 250 \text{ mV}$  with respect to the free corrosion potential at a scan rate of  $1 \text{ mV s}^{-1}$ . Each experiment was

repeated at least three times to check the reproducibility. All electrochemical measurements were performed in a 3.5 % NaCl aqueous solution at 25 °C using a PAR 2263 Potentiostat/Galvanostat.

### 3. RESULTS AND DISCUSSION

#### 3.1 Formation of conversion coatings

##### 3.1.1 Optimal conditions for conversion coatings

The orthogonal experimental analysis was employed to obtain the optimal conditions for conversion coatings. The orthogonal tables for rare earth cerium and stannate were list in table 2 and 3, respectively. AZ31B samples were immersed in the relevant mixes for 1 h and then taken out to give the coated samples. Then, the corrosion current density ( $i_{corr}$ ), which was obtained from Tafel polarization curves for the coated samples after immersion in 3.5 % NaCl for 0.5 h, was used as the evaluating target.

To further analyze the results, the range analysis [20] was conducted to evaluate the significance levels of all the influencing factors and select the optimal level of each factor. For range analysis, the K value and range value (R) were calculated. The K value for each level of a parameter was the average of all the values of samples with the same level. The range value for each factor was the difference between the maximal and minimal values of the three levels. The most significant factor has the highest R value. The mix proportion was selected based on the range analysis.

**Table 4.** The orthogonal experimental analysis results for cerium coating

	A	B	C
K1	880.3	924.3	709.4
K2	718.6	762.1	878.2
K3	796.6	709.1	907.9
R	161.7	215.2	168.8

**Table 5.** The orthogonal experimental analysis results for stannate coating

	A	B	C	D
K1	618.7	346.2	396.0	554.3
K2	275.1	393.3	440.2	355.3
K3	326.2	480.0	383.9	310.5
R	343.6	113.8	56.3	243.8

The statistic analysis of the effect of different factors on corrosion current density for rare earth cerium and stannate coating was summarized in Table 4 and 5, respectively. From Table 4, it is clear that, according to the R-value, the most significant factor for rare earth cerium coating is H<sub>2</sub>O<sub>2</sub>,

followed by temperature which has similar degree of influence with  $\text{Ce}(\text{NO}_3)_3$ . Based on the K value in Table 4, the initial optimal mix can be validated as A2B3C1, that is, the initial optimal mix for rare earth was  $0.01 \text{ mol L}^{-1} \text{ Ce}(\text{NO}_3)_3$  and  $150 \text{ ml L}^{-1} \text{ H}_2\text{O}_2$  at  $40 \text{ }^\circ\text{C}$ .

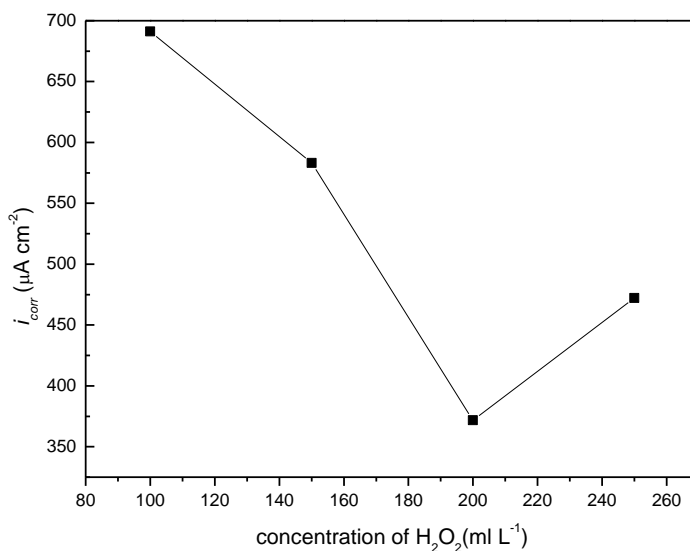


**Figure 1.** Relationship between concentration of  $\text{H}_2\text{O}_2$  and corrosion current density when concentration of  $\text{Ce}(\text{NO}_3)_3$  and experimental temperature were respectively fixed at  $0.01 \text{ mol L}^{-1}$  and  $40 \text{ }^\circ\text{C}$

Because the most significant factor for rare earth cerium coating is  $\text{H}_2\text{O}_2$  and the highest concentration of  $\text{H}_2\text{O}_2$  is  $150 \text{ ml L}^{-1}$  in orthogonal experiments, the effect of increasing  $\text{H}_2\text{O}_2$  concentration on the corrosion resistance of rare earth coating should be further studied. Fig.1 shows the relationship between concentration of  $\text{H}_2\text{O}_2$  and corrosion current density when concentration of  $\text{Ce}(\text{NO}_3)_3$  and experimental temperature were respectively fixed at  $0.01 \text{ mol L}^{-1}$  and  $40 \text{ }^\circ\text{C}$ . As it can be seen from this figure that, the corrosion current density firstly increases with increasing  $\text{H}_2\text{O}_2$  concentration up to  $200 \text{ ml L}^{-1}$  and then decreases, there is a minimum value appears at  $200 \text{ ml L}^{-1} \text{ H}_2\text{O}_2$ . Thus, the optimal conditions for formation of rare earth coating were  $0.01 \text{ M Ce}(\text{NO}_3)_3$ ,  $200 \text{ ml L}^{-1} \text{ H}_2\text{O}_2$  and  $40 \text{ }^\circ\text{C}$ .

From Table 5, it is clear that, according to the R-value, the most significant factor for stannate coating is concentration of  $\text{Na}_2\text{SnO}_3 \cdot 3\text{H}_2\text{O}$ , followed by temperature, the least significant factor is concentration of  $\text{Na}_4\text{P}_2\text{O}_7 \cdot 10\text{H}_2\text{O}$ . Based on the K value in Table 5, the initial optimal mix can be validated as A2B1C3D3, that is, the initial optimal mix for stannate coating was  $0.1 \text{ mol L}^{-1} \text{ Na}_2\text{SnO}_3 \cdot 3\text{H}_2\text{O}$ ,  $0.1 \text{ mol L}^{-1} \text{ Na}_4\text{P}_2\text{O}_7 \cdot 10\text{H}_2\text{O}$  and  $0.1 \text{ mol L}^{-1} \text{ NaOH}$  at  $90 \text{ }^\circ\text{C}$ .

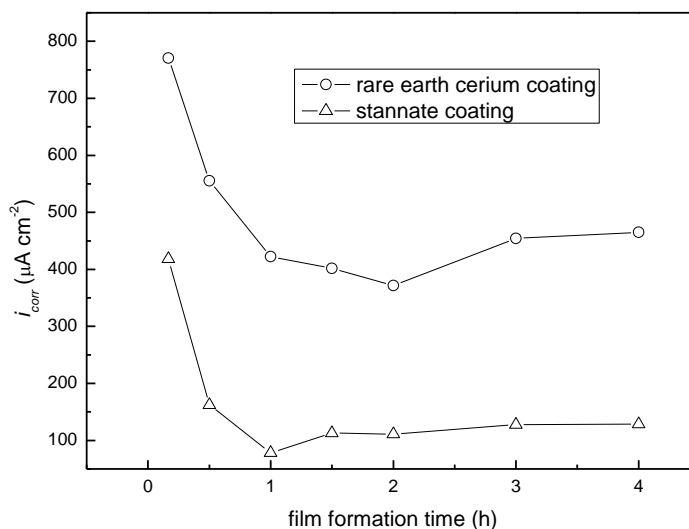
Because the least significant factor is concentration of  $\text{Na}_4\text{P}_2\text{O}_7 \cdot 10\text{H}_2\text{O}$ , the concentration of  $\text{Na}_4\text{P}_2\text{O}_7 \cdot 10\text{H}_2\text{O}$  in the optimal mix for stannate coating can be fixed at  $0.1 \text{ mol L}^{-1}$ . Furthermore, in order to easily control the experiments by water bath heater, the temperature was fixed at  $90 \text{ }^\circ\text{C}$  and not further raised. Therefore, only effects of concentration of  $\text{Na}_2\text{SnO}_3 \cdot 3\text{H}_2\text{O}$  and  $\text{NaOH}$  on the corrosion resistance were subsequently studied in more detail in view of the orthogonal experimental results.

**Table 6.** Effect of concentrations of  $\text{Na}_2\text{SnO}_3$  and  $\text{NaOH}$  on the corrosion resistance of stannate coating

$\text{Na}_2\text{SnO}_3$ (mol L <sup>-1</sup> )	$\text{NaOH}$ (mol L <sup>-1</sup> )	$E_{\text{corr}}$ (V)	$i_{\text{corr}}$ ( $\mu\text{A cm}^{-2}$ )
0.1	0.1	1.517	222.9
0.1	0.15	1.514	113.1
0.2	0.1	1.487	89.8
0.2	0.15	1.473	78.1

In the complementary experiments, 0.1, 0.2 mol L<sup>-1</sup>  $\text{Na}_2\text{SnO}_3 \cdot 3\text{H}_2\text{O}$  and 0.1, 0.15 mol L<sup>-1</sup>  $\text{NaOH}$  were respectively used to ascertain the specific concentrations of  $\text{Na}_2\text{SnO}_3 \cdot 3\text{H}_2\text{O}$  and  $\text{NaOH}$  based on the aforesaid orthogonal analysis. In addition, concentrations of  $\text{Na}_4\text{P}_2\text{O}_7 \cdot 10\text{H}_2\text{O}$  and  $\text{CH}_3\text{COONa} \cdot 3\text{H}_2\text{O}$  were 0.1 mol L<sup>-1</sup>, and the temperature was 90 °C. Table 6 shows the results of the complementary experiments. It is apparent that the corrosion current is the lowest when concentrations of  $\text{Na}_2\text{SnO}_3 \cdot 3\text{H}_2\text{O}$  and  $\text{NaOH}$  are 0.2 and 0.15 mol L<sup>-1</sup>. Therefore, the optimal conditions for stannate coating were 0.2 mol L<sup>-1</sup>  $\text{Na}_2\text{SnO}_3 \cdot 3\text{H}_2\text{O}$ , 0.1 mol L<sup>-1</sup>  $\text{Na}_4\text{P}_2\text{O}_7 \cdot 10\text{H}_2\text{O}$ ,  $\text{CH}_3\text{COONa} \cdot 3\text{H}_2\text{O}$  and 0.15 mol L<sup>-1</sup>  $\text{NaOH}$  at 90 °C.

### 3.1.2. Optimal film formation time

**Figure 2.** Relationship between corrosion current density of conversion coatings and film formation time

As an important influencing factor, the effect of film formation time can not be ignored. To explore the optimal film formation time, the rare earth bath for rare earth cerium coating was fixed at 0.01 mol L<sup>-1</sup>  $\text{Ce}(\text{NO}_3)_3$ , 200 ml L<sup>-1</sup>  $\text{H}_2\text{O}_2$  at 40 °C and the stannate bath for stannate coating was fixed at 0.2 mol L<sup>-1</sup>  $\text{Na}_2\text{SnO}_3 \cdot 3\text{H}_2\text{O}$ , 0.1 mol L<sup>-1</sup>  $\text{Na}_4\text{P}_2\text{O}_7 \cdot 10\text{H}_2\text{O}$ , 0.1 mol L<sup>-1</sup>  $\text{CH}_3\text{COONa} \cdot 3\text{H}_2\text{O}$  and 0.15 mol L<sup>-1</sup>  $\text{NaOH}$  at 90 °C. After immersion in rare earth cerium or stannate bath for different times, the samples were taken out and washed with distilled water, then dried in a desiccator for 6 h. To obtain

the corrosion current density, the pretreated samples were subsequently immersed in 0.35 % NaCl for 0.5 h before Tafel polarization curves were recorded. Fig.2 presents the relationship between corrosion current density of conversion coatings and film formation time. As can be easily seen from this figure, the variation tendency for rare earth cerium and stannate coating are similar, the corrosion current density firstly decreases with increasing film formation time up to certain time and then slightly increases with film formation time higher than the threshold value. And from this figure it is clear that the optimal film formation time for rare earth cerium coating and stannate coating is 2 h and 1 h, respectively.

### 3.1.3. Film preparation

Based on the foregoing studies, the rare earth cerium conversion coating on AZ31B magnesium alloy is formed in rare earth cerium bath containing  $0.01 \text{ mol L}^{-1} \text{ Ce}(\text{NO}_3)_3$ ,  $200 \text{ ml L}^{-1} \text{ H}_2\text{O}_2$  at  $40 \text{ }^\circ\text{C}$  for 2 h, and the stannate conversion coating AZ31B magnesium alloy is formed in stannate bath containing  $0.2 \text{ mol L}^{-1} \text{ Na}_2\text{SnO}_3 \cdot 3\text{H}_2\text{O}$ ,  $0.1 \text{ mol L}^{-1} \text{ Na}_4\text{P}_2\text{O}_7 \cdot 10\text{H}_2\text{O}$ ,  $0.1 \text{ mol L}^{-1} \text{ CH}_3\text{COONa} \cdot 3\text{H}_2\text{O}$  and  $0.15 \text{ mol L}^{-1} \text{ NaOH}$  at  $90 \text{ }^\circ\text{C}$  for 1 h. The composite film coated AZ31B was first performed in rare earth bath at  $40 \text{ }^\circ\text{C}$  for 2 h and then immersed in stannate bath at  $90 \text{ }^\circ\text{C}$  for 1 h.

### 3.2. Corrosion tests of the coatings

Figure 3a and b show the Tafel polarization curves and Nyquist diagrams of the films coated and uncoated AZ31B after immersion in 3.5 % NaCl solution for 0.5 h at  $25 \text{ }^\circ\text{C}$ , respectively. As can be seen from Fig.3a, the corrosion potentials of the films coated AZ31B are shifted to more positive compared to uncoated AZ31B. For the single cerium film, the anodic branch shifts to lower current density region while the cathodic branch does not change obviously, suggesting that the cerium film mainly retards the anodic dissolution of AZ31B; But for the stannate film, both the anodic and cathodic branches shift to lower current density region noticeably, suggesting that the stannate film can restrain both the anodic dissolution of AZ31B and the cathodic deoxidization reaction. Comparing with single stannate or cerium film, the composite film further shifts both the anodic and cathodic branches towards lower current density region clearly, which results in a notably decrease in corrosion current density. The polarization parameters including corrosion potential ( $E_{corr}$  vs. SCE), corrosion current density ( $I_{corr}$ ), Tafel slopes  $\beta_a$  and  $\beta_c$  were calculated by Tafel plots within  $E_{corr}$  vs. SCE  $\pm 150$  mV and listed in Table 7. It is easy to see from this table that, the corrosion current density decreases in the order uncoated AZ31B ( $1009 \text{ } \mu\text{A cm}^{-2}$ ) > single cerium film ( $372 \text{ } \mu\text{A cm}^{-2}$ ) > single stannate film ( $112 \text{ } \mu\text{A cm}^{-2}$ ) > composite film ( $31.6 \text{ } \mu\text{A cm}^{-2}$ ). The corrosion current density values of the anticorrosive multilayered film were much lower than those of other films prepared by single cerium and stannate conversion. This indicates that the composite film has a better corrosive resistance than the single ones.

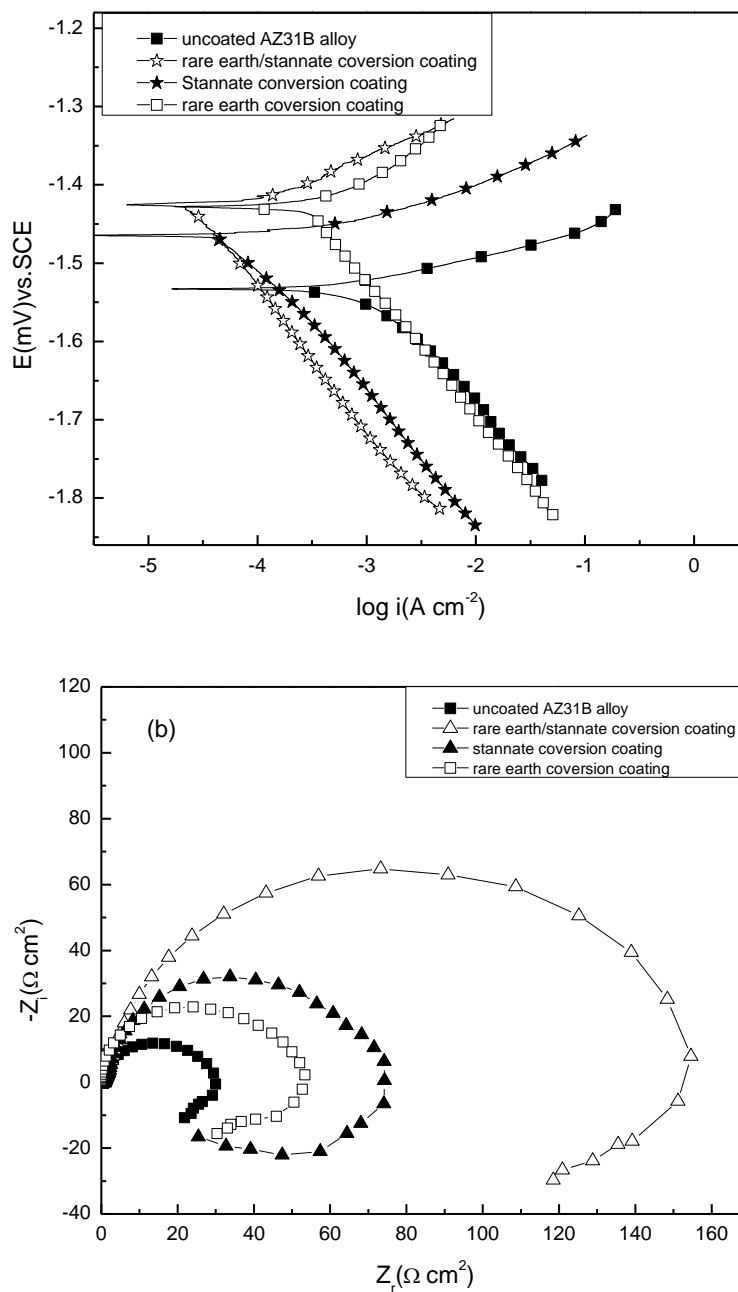


**Figure 3.** Tafel polarization curves (a) and Nyquist diagrams (b) of the films coated and uncoated AZ31B.

From Fig.3b, it is clear that all the EIS are quite similar, all the EIS consists of two loops, one capacitive in the high frequency range (CHF), one inductive loop in the low frequency range (ILF). It is generally agreed that the CHF is always related to the transient resistance and the double layer capacitance of the electrode [21,22], and the inductive loop in the low frequency range is generally attributed to the adsorbed species such as  $Mg(OH)^+$  or  $Mg^+$  [21-25]. It is possible to obtain the oxide film resistance of AZ31B from these loops as presented in Fig. 3b. Comparing the semicircle of CHF, it is easy to see that the loop decreases in the order composite film > stannate film > cerium film >

uncoated AZ31B. The observed increase in the semicircle of CHF for the composite film indicates a progressive enhancement of the corrosion resistance of the coating performed on AZ31B.

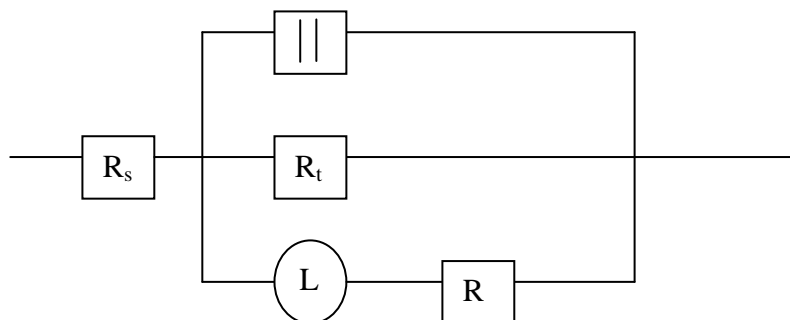


**Figure 4.** Electric equivalent circuit of EIS

The EIS results also were simulated using the equivalent circuit shown in Fig. 4 to pure electronic models that could verify or rule out mechanistic models and enable the calculation of numerical values corresponding to the electrochemical system under investigation [26,27]. In the circuit,  $R_s$  is solution resistance,  $R_t$  is charge transfer resistance and  $C_{dl}$  the double layer capacity associated to the coating film of AZ31B;  $R_L$  and  $L$  describe the low frequency inductive loop.  $R_s$ ,  $R_t$ ,  $C_{dl}$ ,  $R_L$  and  $L$  fitted from the equivalent circuit also were shown in Table 7.

**Table 7.** Electrochemical parameters for pretreated and untreated AZ31B magnesium alloy in 3.5 % NaCl for 0.5 h.

	Tafel polarization				EIS				
	$E_{corr}$ vs. SCE	$I_{corr}$	$\beta_a$	$\beta_c$	$R_s$	$R_{ct}$	$C_{dl}$	$R_L$	$L$
	mV	$\mu A cm^{-2}$	mV dec <sup>-1</sup>	mV dec <sup>-1</sup>	$\Omega cm^2$	$\Omega cm^2$	$\mu F cm^{-2}$	$\Omega cm^2$	H•c m <sup>2</sup>
Non-coating	-1532	1009	146	39	0.55 86	26.93	245	34.69	44.0 1
Cerium coating	-1432	372	184	87	0.54 98	49.75	54.8	38.63	59.1 6
Stannate coating	-1473	112	177	41	0.60 46	75.83	78.7	32.76	36.8 2
Composite coating	-1442	31.6	188	54	0.81 93	171	140	32.18	125. 3

From this table it also can be found that,  $R_{ct}$ , the charge transfer resistance which represents the corrosion resistance of the coating, decreases in the order composite film > stannate film > cerium film > uncoated AZ31B, suggesting the corrosion resistance of the composite film is much better than single ones. This result is well in agreement with that from Tafel polarization.

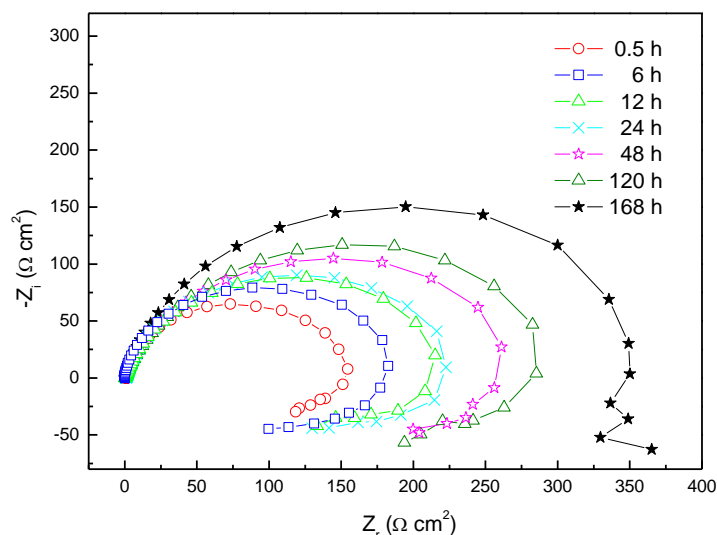


**Figure 5.** EIS of the composite film coated on AZ31B magnesium alloy immersed in 3.5% for different times at 25 °C.

The results obtained from Tafel polarization and EIS show that the composite film has better corrosion resistance. To further elucidate the validity of the composite film, the composite film as a function of different immersion time in 3.5 % NaCl solution at 25 °C was recorded by EIS and shown in Fig.5. From this figure, it is apparent that, the shapes of the impedance diagram are quite similar at different times, and the immersion time increases the size of the capacitive in the high frequency range significantly, suggesting that the film becomes more protective with increasing immersion time. The composite film still has well protective capability even after immersion in 3.5% NaCl for 168 h. Therefore, combination of cerium and stannate may be an effective strategy for improving the anticorrosion performance of chemically treated magnesium alloys.

### 3.3. XRD and SEM studies

The SEM microstructures of AZ31B surfaces treated with different methods were shown in Fig.6. In order to easily compare, the SEM micrograph of the AZ31B substrate after immersion in distilled water at 25 °C was shown Fig.6a, it is clear that there are no obvious corrosion products appeared on AZ31B substrate, parallel features in this figure can be associated with abrading scratches. On the contrary, as can be seen from Fig.6b, a large amount of substances present and form a thick layer on AZ31B surface treated with rare earth cerium, but the film is inhomogeneous, there are some sunken places and tiny crevices appeared in the film, some aggressive ions can penetrate these crevices and cause the dissolution of AZ31B, suggesting that single cerium conversion film can retard the corrosion somewhat. XRD pattern of the film formed on AZ31B surface dealt with cerium reveals that  $\text{CeO}_2$  and  $\text{Mg}(\text{OH})_2$  are the main corrosion products (Data not shown here).

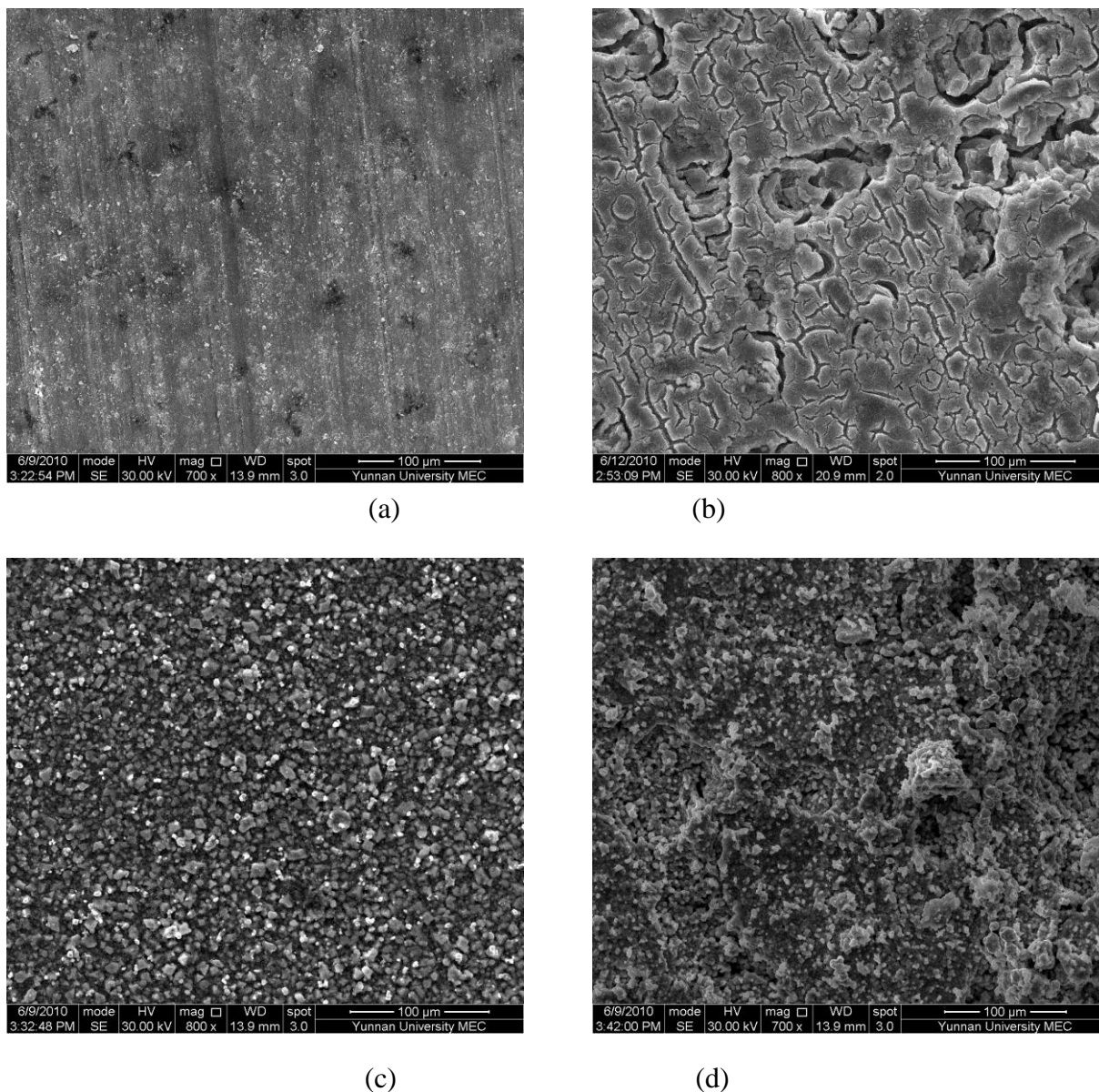


**Figure 6.** SEM examinations of AZ31B surfaces (a) AZ31B substrate, (b) cerium conversion film, (c) stannate conversion film, (d) combinational film of cerium and stannate.

Fig.6c clearly shows that the stannate conversion film is composed of large amount of small particles and has notably high integrity, which occupies the active sites of AZ31B and forms a protective film, so corrosion of AZ31B can be suppressed by formation of stannate conversion film. However, some small ions such as  $\text{Cl}^-$  can get across the interval among the particles, suggesting that corrosion of AZ31B still can occur in some media. XRD pattern of the film formed on AZ31B surface dealt with stannate reveals that  $\text{MgSnO}_3$ ,  $\text{MgSnO}_3 \cdot 3\text{H}_2\text{O}$  and  $\text{Mg}(\text{OH})_2$  are the main corrosion products (Data not shown here). Moreover, comparing with the film treated with single cerium, it is apparent from Fig.6d that the composite film formed on AZ31B by a combination process of cerium and stannate consists of multilayer film, especially, the sunken places and tiny crevices in single

cerium conversion coating are covered with lot of particles. The deposit particles further makes up for defects of single cerium conversion coating.

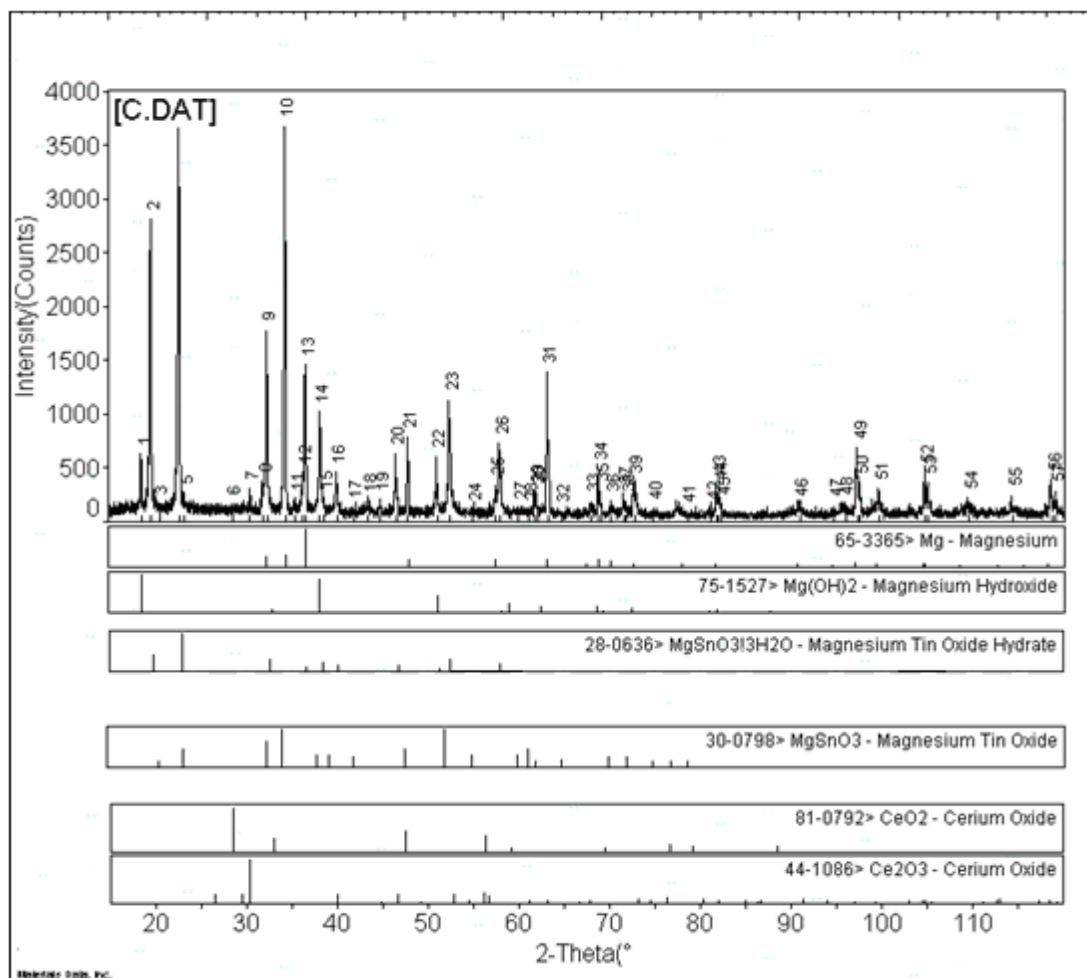
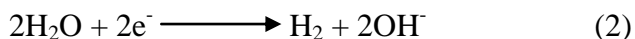


**Figure 7.** XRD patterns of the composite film coated on AZ31B.

So the corrosion resistance can be further improved by the composite coating. Fig.7 gives the XRD results of the composite coating, peaks at 9, 10, 13, 21, 26, 31 and 34 can be attributed to magnesium substrate, peaks at 1, 14, 30, 39 and 43 are assigned to  $Mg(OH)_2$ , peaks at 6, 10, 21, 26 and 28 are due to  $CeO_2$ , peaks a 2, 4, 9, 16, 23 and 26 can be attributed to  $MgSnO_3$ , peaks at 2, 4, 9, 10, 13, 14, 17, 21, 23, 24, 29, 31, 34, 39 are corresponding to  $MgSnO_3 \cdot 3H_2O$ . Thus it is easy to see that  $MgSnO_3$ ,  $MgSnO_3 \cdot 3H_2O$ ,  $Mg(OH)_2$  and  $CeO_2$  present in the corrosion products, which further suggests that the composite coating is the interaction result of rare earth cerium and stannate. From XRD and SEM results, the composite film could be formed by following manner;  $CeO_2$  and  $Mg(OH)_2$  as precursors are initially formed on AZ31B alloy by cerium chemical conversion, then, stannate chemical conversion begins to come into being on the precursor film, resulting in the formation of crystalline  $MgSnO_3$ ,  $MgSnO_3 \cdot 3H_2O$  and  $Mg(OH)_2$ .

#### 4. FORMATION MECHANISM OF THE COMPOSITE FILM

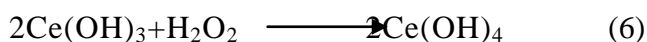
Generally speaking, the anodic dissolution of AZ31B magnesium alloy in solution is always accompanied by the cathodic hydrogen evolution [28].



Therefore, countless electrochemical cells begin to form on the surface of AZ31B. Then cations, e.g.  $\text{Mg}^{2+}$ , will migrate towards to the cathodic areas, at the same time anions, e.g.  $\text{OH}^-$  will migrate towards to the dissolution sites. Accordingly,  $\text{Mg(OH)}_2$  produces close to the anodic sites.



On the other hand, the  $\text{OH}^-$  produced in reaction (2) leads to pH value increase at the interface between the substrate and the solution. Once  $\text{Ce(NO}_3)_3$  and  $\text{H}_2\text{O}_2$  presents in solution, the following reactions also will occur.

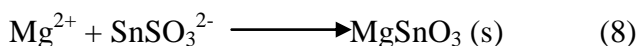


$\text{Ce(OH)}_4$  is unstable which easily dehydrates to  $\text{CeO}_2(\text{s})$  [13]



So  $\text{Mg(OH)}_2$ ,  $\text{CeO}_2(\text{s})$  will be precipitated on the AZ31B surface which can retard the dissolution of AZ31B somewhat. This is in agreement with XRD results of AZ31B pretreated with rare earth cerium bath.

Once AZ31B is immersed in stannate bath, reactions 1-4 also take place; in addition,  $\text{Mg}^{2+}$  also can react with stannate ions forming indissoluble magnesium stannate which precipitates on the surface of AZ31B. This also results in a considerable decrease in the corrosion of AZ31B.



Considering the above discussion, we can draw a conclusion that, when the AZ31B samples are treated by rare earth bath, reactions 1-7 will take place, which results in the formation of rare earth cerium film. As the coating formation proceeds, the substrate surface is gradually covered with cerium oxide and magnesium hydroxide, but the film is unevenly distributed on AZ31B attributed to the electrochemical corrosion. The coating retards the corrosion of AZ31B somewhat. However, when the samples pretreated by rare earth bath are immersed in stannate bath again, some aggressive ions can penetrate the cerium coating and cause the dissolution of AZ31B, which brings some  $Mg^{2+}$  ions into solution, consequently, reactions 8 and 9 will occur and form an indissoluble magnesium stannate layer on cerium coating, which further inhibits the dissolution of AZ31B magnesium alloy. Due to the sequential cooperation between rare earth cerium and stannate, a multilayer film composed of cerium oxide, magnesium stannate compounds and magnesium hydroxide forms on AZ31B surface, which shows much higher corrosive resistance than the film coated by single cerium or stannate.

## 5. CONCLUSIONS

1. Orthogonal experimental analysis was used to select the optimal conditions for formation of single rare earth cerium or stannate conversion coatings on AZ31B magnesium alloy. The rare earth cerium conversion coating is formed in rare earth cerium bath containing  $0.01 \text{ mol L}^{-1} \text{ Ce}(\text{NO}_3)_3$ ,  $200 \text{ ml L}^{-1} \text{ H}_2\text{O}_2$  at  $40 \text{ }^\circ\text{C}$  for 2 h, and the stannate conversion coating is formed in stannate bath containing  $0.2 \text{ mol L}^{-1} \text{ Na}_2\text{SnO}_3 \cdot 3\text{H}_2\text{O}$ ,  $0.1 \text{ mol L}^{-1} \text{ Na}_4\text{P}_2\text{O}_7 \cdot 10\text{H}_2\text{O}$ ,  $0.1 \text{ mol L}^{-1} \text{ CH}_3\text{COONa} \cdot 3\text{H}_2\text{O}$  and  $0.15 \text{ mol L}^{-1} \text{ NaOH}$  at  $90 \text{ }^\circ\text{C}$  for 1 h. Accordingly, the anticorrosive composite film coated AZ31B was first performed in rare earth bath at  $40 \text{ }^\circ\text{C}$  for 2 h and then immersed in stannate bath at  $90 \text{ }^\circ\text{C}$  for 1 h.

2. Combination of cerium and stannate may be an effective strategy for improving the anticorrosion performance of chemically treated magnesium alloys. The composite film is a multilayer film composed of cerium oxide, magnesium stannate compounds and magnesium hydroxide.

3. Both rare earth cerium coating and stannate coating can retard the dissolution of AZ31B magnesium alloy somewhat, but the composite film by a combination process of rare earth cerium and stannate shows much higher corrosive resistance than any single ones. The corrosion resistance of the composite film also shows good anticorrosive performance even after immersion in 3.5% NaCl for 168 h.

## ACKNOWLEDGEMENT

This work was financially supported by Chinese Natural Science Foundation under the Grant Nos. 51161025, 21162036, 50761007, and 20762014.

## References

1. W. Liu, F. Cao, L. Chang, Z. Zhang, J. Zhang, *Corros. Sci.* 51(2009)1334.
2. Y.H. Wei, L.J. Yang, L.F. Hou, Y.W. Guo, B.S. Xu, *Eng. Fail. Anal.* 16(2009) 19.

3. T. Ishizaki, R. Kudo, T. Omi, K. Teshima, T. Sonoda, I. Shigematsu, M. Sakamoto, *Mater. Lett.* 68(2012)122
4. X. Wang, X. Zeng, G. Wu, *J. Alloy Compd.* 437(2007)87.
5. C.S. Lin, S.K. Fang, *J. Electrochem. Soc.* 152(2005)B54.
6. C.S. Lin, C.Y. Lee, W.C. Li, Y.S. Chen, G.N. Fang, *J. Electrochem. Soc.* 153(2006)B90.
7. T. Ishizaki, R. Kudo, T. Omi, K. Teshima, T. Sonoda, I. Shigematsu, M. Sakamoto, *Electrochim. Acta* 62 (2012) 19.
8. X. Yang, F. Pan, D. Zhang, *Appl. Surf. Sci.* 255(2008)1782.
9. M.W. Kendig, R.G. Buchheit, *Corrosion* 59(2003)379.
10. A.L. Rudd, C.B. Breslina, F. Mansfeld, *Corros. Sci.* 42 (2000)275.
11. M. Dabala, K. Brunelli, E. Napolitani, M. Magrini, *Surf. Coat. Technol.* 172 (2003) 227.
12. M.F. Montemor, A.M. Simões, M.G.S. Ferreira, M.J. Carmezim, *Appl. Surf. Sci.* 254 (2008) 1806
13. F. El-Taib Heakal, O.S. Shehata, N.S. Tantawy, *Corros. Sci.* 56 (2012) 86.
14. M.A. Gonzalez-Nunez, C.A. Nunez-Lopez, P. Skeldon, G.E. Thompson, H. Karimzadeh, P. Lyon, T.E. Wilks, *Corros. Sci.* 37 (1995)1763.
15. M.A. Gonzalez-Nunez, P. Skeldon, G.E. Thompson, H. Karimzadeh, *Corrosion* 55 (1999) 1136.
16. C.S. Lin, H.C. Lin, K.M. Lin, W.C. Lai, *Corros. Sci.* 48 (2006) 93.
17. H.X. Jin, R.C. Wang, C.Q. Peng, Y. Feng, K. Shi, B. Chen, *Chin. J. Nonferrous Met.* 21(2011)2049
18. S.A. Salman, R. Ichino, M. Okido, *Chem. Lett.* 36 (2007)1024.
19. H.H. Elsentriecy, K. Azumi, H. Konno, *Electrochim. Acta* 53 (2007) 1006.
20. Z. Ge, Z.L. Gao, R.J. Sun, L. Zheng, *Constr. Build. Mater.* 31 (2012) 289.
21. G. Song, A. Aterens, X. Wu, B. Zhang, *Corros. Sci.* 40(1998) 1769.
22. G. Baril, C. Blanc, N. Pébère, *J. Electrochem. Soc.* 148(2001)B489.
23. M. Anik, G. Celikten, *Corros. Sci.* 49 (2007) 1878.
24. G. Song, A. Aterens, D.S.T. Jonh, X. Wu, J. Nairn, *Corros. Sci.* 39 (1997) 1981.
25. G. Baril, N. Pébère, *Corros. Sci.* 43 (2001) 471.
26. Q. Qu, S. Jiang, W. Bai, L. Li, *Electrochim. Acta* 52 (2007) 6811.
27. W.A. Badawy, K.M. Ismail, A.M. Fathi, *Electrochim. Acta* 51 (2006)4182.
28. Q. Qu, J. Ma, L. Wang, L. Li, W. Bai, Z. Ding, *Corros. Sci.* 53 (2011)1186.